Modeling silver clusters-hydrocarbon interactions: A challenge for SCC-DFTB

Camille Alauzet, Fernand Spiegelman, Aude Simon

Modeling silver clusters-hydrocarbon interactions: a challenge for SCC-DFTB

Camille Alauzet, Fernand Spiegelman, Aude Simon

Laboratoire de Chimie et Physique Quantiques (LCPQ), FeRMI Institute, UMR5626 Université de Toulouse [UT3 Paul Sabatier] & CNRS, 118 Route de Narbonne, 31062 Toulouse, France

Abstract

This work examines the reliability of the Self Consistent Charge Density Functional based Tight Binding (SCC-DFTB) scheme to derive geometrical and thermochemistry observables for complexes and clusters made of Ag, C and H atoms. In addition to the currently available DFTB parameterization DFTB$^{\mathrm{hyb}}$, it proposes a new SCC-DFTB parameterization based on DFT Slater Koster integrals and recalibrated on atomic pairs MRCI calculations for clusters made of Ag, C and H atoms. Two sets of parameters were determined, one for restricted open shell SCC-DFTB, the other for spin-polarized SCC-DFTB. These two new sets of parameters, namely DFTB$^{\gamma}$ and DFTB$^{\gamma pol}$ respectively, along with DFTB$^{\mathrm{hyb}}$, are first tested on Ag_n, Ag_nC and Ag_nH clusters. A key issue being the transferability of such parameters on different types of Ag-X bonds, the three sets of parameters are then tested on $Ag_mC_nH_p$ (m=1-3, n=2, p=0-2) complexes involving covalent and π metal-ligand bonds. The particular case of naphthalene $C_{10}H_8$ as a π-ligand is also investigated. In general, with respect to DFTB$^{\mathrm{hyb}}$results, using DFTB$^{\gamma}$ parameters leads to an improvement of geometries and energetics. In the case of $Ag_nC_{10}H_8$ clusters, the role of dispersion is evidenced. However, in a few cases, the geometries may distort due to a questionable description of charge transfer with DFTB$^{\gamma}$ and DFTB$^{\gamma pol}$. The spin-polarized version of SCC-DFTB is suited to correctly describe open-shell species with more than one unpaired electron in their ground electronic state but is shown not to improve the results otherwise.

Keywords: clusters, organometallics, DFTB, parameterization

1. Introduction

Silver nanoparticles have sustained a lot of interest due to their optical, electronic, biological and catalytic properties [1] that make them attractive for many technological and industrial applications [2]. Noble metal nanoclusters indeed possess high biocompatibility, chemical stability, low toxicity and low photo-bleaching, which make them adapted as constituents of biosensors [3]. Their physical and chemical properties can be modified by functionalization as for instance the functionalization of silver nanoclusters by graphene [4], leading to composite materials with new properties that can be exploited for industrial purposes.

In a more fundamental context, silver was used in order to study the impact of the presence of a metal seed on dust formation in an environment in which the key elements involved in stardust formation (C, H, O, Si) are already present [5]. In this context, the formation of complexes of silver with hydrocarbons was observed in the gas phase under different conditions : in a laser vaporisation source after reaction of laser ablated silver and acetylene (1% in He gas) and in cold plasma after reaction of sputtered silver with pulsed hexamethyldisiloxane (HMDSO). The formation of large hydrocarbons corresponding to the chemical composition of anthracene and pyrene, was also observed. A complex organometallic - catalytic - chemistry is assumed to occur, triggered by an organometallic seed that could be Ag_n-C≡CH. At a larger scale, scanning electron microscopy (SEM) images of the plasma after reaction show the formation of a dust structure with two phases, organosilicon dust and silver nanoparticles organized in a "raspberry-like" structure in a plasma after reaction of acetylene with silver in the presence of HMDSO. The work presented in this paper enters the general goal of aiming to understand this reactivity and this phase separation at the subnanometer scale by means of quantum chemical calculations.

In order to describe chemical reactions between Ag, C and H, and eventually Si and O, electronic structure needs to be explicitely described. The chemical complexity of such systems prevents the use of reactive force fields. Given the complexity of the potential energy surfaces (PES) and the targeted size of the systems (a few hundreds of atoms), the use of common DFT methods seems prohibited, at least in the context of statistically meaningful intensive simulations such as molecular dynamics or Monte Carlo schemes.

A good compromise between efficiency and reliability is the self-consistent charge density functional based tight binding (SCC-DFTB) [6] scheme, which makes the bridge between molecular level with a few atoms and nanoscale. Several studies were dedicated to the description of silver clusters in their electronic ground state using an adjusted SCC-DFTB hamiltonian where the Ag-Ag DFTB hamiltonian matrix elements of the hyb-0-2 set of parameters (available from www.dftb.org) were scaled by 0.90 in order to improve structural features and energetics [7, 8, 9]. Heat capacities for Ag_{20} and Ag_{55} were also derived from parallel tempering molecular dynamics simulations [10].

Silver nanoparticles are also interesting for their plasmonic properties, and this has motivated the simulations of the optical spectra of several types of silver clusters using the Time-Dependent (TD-) DFTB method using the hyb-0-2 set of parameters. For instance, the optical properties of silver nanoparticles dimers were studied using the linear-response TD-DFTB methodology [11] and the optical absorption spectra of silver and gold nanoclusters were simulated using real-time (RT) DFTB dynamics [12].

To our knowledge, DFTB studies of mixed clusters involving Ag and C,H,Si and/or O elements and of their reactivity are scarce. Studies of geometric and electronic properties of silicon clusters doped by a silver atom $AgSi_n$ (n=1-15) were determined using the random search algorithm with the DFTB hamiltonian, the 10 final most stable isomeric structures were further locally optimized at the DFT level of theory [13]. The influence of Si-doping on small silver clusters (neutral, cationic and anionic) on their optimical properties was studied using DFTB to optimize the geometry of the clusters and linear-response TD-DFTB to simulate their UV-visible spectra. [14] In this study, the gap between the highest occupied and lowest unoccupied molecular orbitals and therefore the optical spectrum were shown to vary significantly under Si doping, enabling flexible tuning of the chemical and optical properties of silver clusters. Recently, real-time RT-DFTB dynamics of H_2 adsorbed on octahedral nanoparticles of silver Ag_nH_2 (and gold Au_nH_2) with n ranging from 19 to 489 was performed to give insights into plasmon-driven H_2 dissociation [15].

The aim of the present work is to assess the ability of SCC-DFTB (usually named DFTB in the rest of the manuscript) in its restricted open-shell [6] and in its spin-polarized version [16], including or not Grimme dispersion interactions [17] to describe the geometrical and energetic properties of clus-

ters and species including Ag, C and H. Restricted open-shell SCC-DFTB without spin-polarization can be used for most clusters, which are in low spin states, either singlet or doublet. A correct account of thermochemistry requires both correct global energetic data, such as the cohesive energies of the global entities, but also relative energies corresponding to reactive scenarii, such as the dissociation or binding energies. We show that the currently available parameters (named DFTB$^{\mathrm{hyb}}$hereafter) are not fully satisfactory. In order to contribute to parameterization improvement, we explore a new DFTB parameterization scheme for the X,Y atomic pairs (X,Y=Ag, C, H) based on DFT extracted Slater Koster (SK) and overlap integrals, readjusted *vs* pair potentials determined from multireference configuration interaction (MRCI) calculations [18]. The methodology is detailed in Section 2.

These new sets of parameters are tested on different types of clusters possessing covalent, partly ionic or van der Waals interactions: clusters perturbed by the adsorption of a carbon atom Ag_nC or a hydrogen atom Ag_nH, small $Ag_mC_nH_p$ (m=1,2, n=2, p=0-2) clusters and Ag_n-$C_{10}H_8$ (n=1-8) complexes, that could be reactive intermediates in the reaction of acetylene with silver clusters [5]. Comparison between the structures and energetics obtained with the new sets of parameters (named hereafter DFTB$^{\gamma}$ and DFTB$^{\gamma pol}$) and with the hyb-0-2 of parameters (DFTB$^{\mathrm{hyb}}$) is discussed. Results are compared with DFT data either from the literature or computed in the present work that are considered as reference data. All results are presented and discussed in Section 3.

2. Methodology

We first briefly remind the basics of the SCC-DFTB methodologies used in the present work in subsection 2.1. We then explain the new parameterization scheme proposed in this work in subsection 2.2. Finally, computational details are provided in subsection 2.3.

2.1. The SCC-DFTB hamiltonian

The principles of the DFTB and SCC-DFTB methods are detailed in two fundamental articles [19, 6]. In this work, we use both the restricted open-shell SCC-DFTB [6] and the spin-polarized version [16] also including

dispersion corrections [17] detailed hereafter.

Briefly, the Kohn-Sham (KS) energy is developed following a 2^{nd} order Taylor expansion with respect to the fluctuations of the electronic density around a reference density ρ_0, ρ_0 corresponding to the superposition of atom-like densities centered on each nucleus ($(\rho(\mathbf{r}) = \boldsymbol{\rho_0}(\mathbf{r}) + \delta\rho(\mathbf{r})$). Charge density fluctuations $\delta\rho(\mathbf{r})$ are decomposed into contributions per atom A and possibly angular momentum l and integrals involving three- and four-center contributions are neglected. In the spin-polarized hamiltonian, the magnetisation density is also expressed as a fluctuation around a reference magnetisation density $m(\mathbf{r}) = \mathbf{m_0}(\mathbf{r}) + \delta\mathbf{m}(\mathbf{r})$ (see ref. [20] for details of the spin-polarized SCC-DFTB scheme). Hence, the total energy becomes :

$$\begin{aligned} E^{SCC-DFTB} &= \sum_{\sigma=\alpha,\beta} \sum_{i}^{occ} n_{i,\sigma} \langle \psi_{i,\sigma} | \widehat{H}[\rho_0] | \psi_{i,\sigma} \rangle + \frac{1}{2} \sum_{A,B}^{N} \sum_{l \in A} \sum_{l' \in B} \gamma_{AlBl'} \delta q_{Al} \delta q_{Bl'} \\ &+ \frac{1}{2} \sum_{A}^{N} \sum_{l \in A} \sum_{l' \in A} p_{Al} p_{Al'} W_{All'} + E^{disp} + E^{rep} \end{aligned} \tag{1}$$

-(i)- the first term is the band energy where $\psi_{i,\sigma}$ are the KS spin orbitals (the KS molecular orbitals in the non spin-polarized case), $\widehat{H}[\rho_0]$ is the monoelectronic Hamiltonian at the reference density and $\mathrm{n}_{i,\sigma}$ is the molecular (spin-)orbital occupation number. Only valence electrons are described explicitly and the KS molecular orbitals are developed on a minimal basis set of atomic orbitals,
-(ii)- the second term is the Coulomb energy (or second order term) expressed as a function of orbital Mulliken atomic charges and of a parameterized γ matrix whose elements $\gamma_{AlBl'}$ are functions depending on the interatomic distance and on the atomic Hubbard parameters, possibly shell-resolved U_{Al},
-(iii) the third term is the spin-polarization contribution, based on a one-center approximation. p_{Al} is the difference between the spin up and spin down populations on atom A with angular momentum l. The $W_{All'}$ spin constants are determined similarly to the Hubbard terms from atomic DFT calculations [20, 21],
-(iv)- the fourth term contains the Grimme dispersion corrections [22] asociated with the Becke Johnson damping function (D3-BJ) [23] which avoids

short-range divergence.
-(v)- the short-distance repulsive term E^{rep} is expressed as a function of two-body interactions.

Regarding the SCC-DFTB parameterization, the off-diagonal elements of the KS and overlap matrices in the atomic basis are commonly interpolated from DFT calculations on a distance grid on atomic pairs. The repulsive term E^{rep} is then commonly determined by an analytical fit of the difference:

$$E^{rep}(\mathbf{R}) = \mathbf{E^{DFT}_{ref}}(\mathbf{R}) - \mathbf{E^{DFTB}_{elec}} \tag{2}$$

where E^{DFTB}_{elec} is the electronic part of the above energy, including second order terms, dispersion contributions, and the spin-polarization term (in the spin-polarized vesion).

2.2. Parameterization based on MRCI calculations

Almost all previous DFTB parameterizations have been developed based on DFT calculations only. Retaining only two-atom integrals, the SK integrals, namely the hamiltonian and the overlap integrals, are calculated as expectation values at a given geometry in the basis of frozen atomic orbitals, the sum of the atomic densities being the reference to calculate the mean field part. The most delicate stage of the parameterization concerns the repulsive part (possibly complemented by an additive Van der Waals contribution), which may be extracted either from total energy DFT reference calculations or to reproduce reference material data on various molecules or on bulk systems. The quality of the data obviously also depends on the reference DFT calculations and in particular on the functional used. Actually, DFTB parameters are available for H-H,C-H and C-C pairs (mio set of parameters [6]) and Ag-Ag, Ag-H Ag-C pairs (hyb-0-2 set of parameters[1]) but the hyb-0-2 set provides overbinding for Ag-Ag, Ag-H and Ag-C pairs (see Table S1). This may significantly alter the relevance of investigations concerned with reaction enthalpies and energetics in general.

We have then followed a different methodology to extract parameters consistent with high quality calculations of the diatomic pairs consisting in:

[1]https://dftb.org/parameters/download/hyb/hyb-0-2-cc

1. MRCI determination of atomic pair potentials, almost reproducing experimental molecular data on those pairs (see Table S1),
2. Extraction of (i) the SK integrals (integrals of the Kohn-Sham hamiltonian in the minimal DFTB basis set) from DFT-PBE atomic and molecular calculations at the reference density. The atomic orbital confinement parameters (confinement radii and power values rounded to integer numbers) and of (ii) the l-dependant on-site Coulomb integrals, as tabulated by Wahiduazzan et al. [24]. The standard SK parameterization may however presents overbinding which already affects the medium and long range distance regions, namely distance regions where the repulsive contribution is supposed to vanish. In order to cure this long distance problem, for each molecule, we have reduced the SK and overlaps integrals using a common damping function for the hamiltonian and the overlap integrals. Details are given in the Supplementary Information. The parameters of the damping expression were determined via a fit of the electronic DFTB potential (not including the repulsive contribution) to the MRCI potential beyond a given radius r_0 longer than the equilibrium distance. The expressions and parameters of the damping functions are reported in Tables S1 and S2 for DFTB$^{\gamma pol}$ and DFTB$^{\gamma}$ sets of parameters respectively.
3. Determination of the repulsive part as the difference between the MRCI energy and the repulsion-less DFTB energy (after dispersion was removed for both) and finally fitting via spline functions for adaptation to one of the conventional format compatible with the DFTB^{+} package [25].

The above procedure is achieved hereafter both the ROS DFTB scheme and the spin-polarized DFTB scheme. In the restricted scheme, fitting to the MRCI results cures the overbinding of restricted schemes dissociating above the neutral open shell fragments (atoms), while spin multiplicity splitting specifically due to exchange contributions is not accounted for. The procedure is also carried out using the presumably better grounded spin-polarized DFTB hamiltonian derived from the UKS (unrestricted) DFT treatment, allowing for symmetry broken solutions at dissociation and accounting for spin multiplicity splitting. Figure 1 illustrates the various contributions to the parameterization scheme in the case of C-C in the spin-polarized version for dissociation into C(^{3}P)+C(^{3}P).

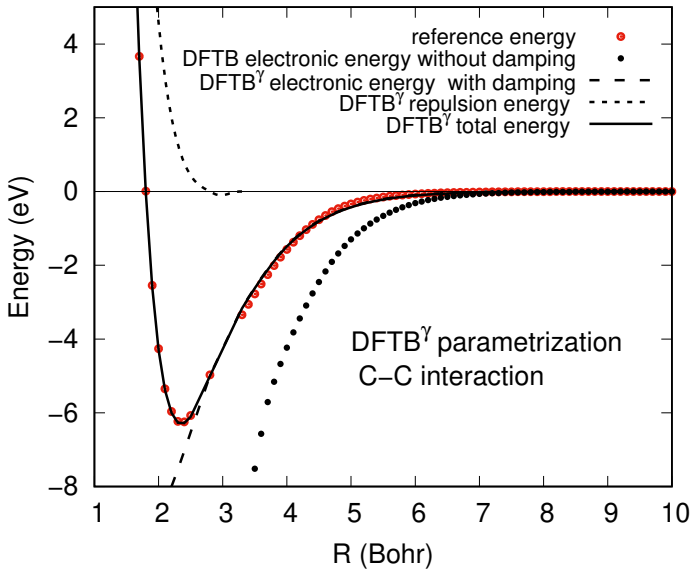

Figure 1: Potential energy contributions to the DFTB$^{\gamma pol}$ parameterization scheme as a function of the interatomic distance R (C-C) interaction).

2.3. Computational details

MRCI calculations. Calculations for step 1 were conducted at the MRCI level [18] with the MOLPRO package[26] using large spdfg basis sets for H and C Gaussian Type Orbital (GTO) based on the exponents of the aug-cc-pv6z set with no contraction. In the case of Ag, a large core effective potential (ECP46SDF from the Stuttgart group [27]) was used, with a 9s7p6d5f5g GTO basis, complemented by a cor-polarization operator [28]. The MRCI calculation is based on an initial valence complete active space self consistent field (CASSCF) calculation, while the generating space of the MRCI calculations systematically involves one more orbital in each orbital symmetry manifold. The calculations were made with the MOLPRO package [26], using the D_{2h} symmetry group for homonuclear species and the C_{2v} group for heteronuclear species. Diatomic potentials were calculated on a wide range of distance, from inner regions up to dissociation. This provides very accurate molecular reference data, very close to the experimental values, as can be seen in Table S1. A special comment should be made about AgC, the only diatomics for which no experimental information is available. The present MRCI calculation with a large core polarization complemented by CPP pro-

vides a dissociation energy of 1.59 eV for the $^4\Sigma^+$ state. This is somewhat smaller that the 2.04 eV value provided by a CCSD(T) coupled cluster calculation reported by Li et al. [29] using a smaller core effective potential, namely the ECP28MWB potential of the Stuttgart group with a [6s5p3d1f] basis set. In order to check further and get an accurate determination of the AgC potential, we have carried out complementary CCSD(T) calculations with the previous large core effective potential ECP46SDF (complemented by CPP) , but also with smaller core pseudopotentials ECP28MWB and ECP28MDF of the Stuttgart group and finally all-electrons calculations of the AgC molecule, with very large basis sets (see Supplementary Information, Figure S1 and Table S3). The result is that all of them provide very similar results, with R_e in the range 2.01-2.02 Åand D_e in the range 1.55-1.59 eV. The ECP46+CPP/MRCI potential was thus retained (Re=2.02 Å, D_e=1.59 eV) for AgC, in consistency with the other diatomic pairs, as the reference calculation.

DFTB calculations. All DFTB calculations were performed with the DFTB$^+$ [25] package. Regarding spin-polarized calculations and Grimme dispersion corrections, the values taken for spin coupling constants and dispersion damping function coefficients are specified in the Supplementary Information.

DFT calculations. In order to assess the validity of the different DFTB hamiltonians, we optimized the geometries of a variety of clusters and determined their energetic properties. Geometry optimizations were also performed at the DFT level of theory using the Gaussian16 suite of programs [30]. Two types of functionals were used : (i) the B3LYP hybrid functional with Grimme dispersion corrections complemented by the Becke Johnson damping function (D3-BJ) [23]. Based on the comparison between the infrared pre-dissociation (IRPD) spectrum of Ag-Naphthalene$^+$ [31] and the computed harmonic absorption spectrum [32], the B3LYP-D3BJ functional was considered to correctly describe the PES of Ag-Naphthalene$^+$ [32]. (ii) the ωB97XD hybrid range separated functional, which also includes empirical dispersion and long-range corrections [33]. This functional was used to describe $Ag_mC_nH_p$ complexes in a previous work [5]. The cc-pvtz basis set for C and H was used while the 4s, 4p, 4d, and 5s electrons of Ag are described using a [6s5p3d] basis set [34] associated to the Stuttgart relativistic effective core potential (ECP) [35] that describes the 28 remaining core elec-

trons. Basis sets and ECP were obtained from the Basis Set Exchange [36].

Energetic data. The following energetic data were computed for the different types of clusters:
Cohesion energies ($E^{cohes.}$) and metal-ligand binding energies (BEs) defined as

$$E^{cohes.}(Ag_mC_nH_p) = mE(Ag) + nE(C) + pE(H) - E(Ag_mC_nH_p) \quad (3)$$

$$BE(Ag_mC_nH_p) = E(Ag_m) + E(C_nH_p) - E(Ag_mC_nH_p) \quad (4)$$

In the definition of $E^{cohes.}$ and BE, the energies refer to the energies of the optimized structures.

In some relevant case, the numerical values of the second-order derivatives of the total energy

$$\frac{d^2E}{dm^2} = \frac{1}{2}(E(Ag_{m+1}C_nH_p) + E(Ag_{m-1}C_nH_p) - 2E(Ag_mC_nH_p)) \quad (5)$$

are computed. This quantity enables us to identify notably stable structures corresponding to a large value of $\frac{d^2E}{dm^2}$, commonly referred to as "magic number" structures.

3. Results and discussion

We remind that the results obtained with the mio/hyb-2-0 set of parameters will be labelled $DFTB^{hyb}$ while those resulting from the parameterization proposed in this work will be labelled $DFTB^{\gamma}$ for restricted open-shell (ROS) DFTB without spin-polarization or $DFTB^{\gamma pol}$ for spin-polarized DFTB calculations. The spin constants of the $DFTB^{hyb}$ version are those provided with or included in the $DFTB^{hyb}$ skf files. The spin constants used in the $DFTB^{\gamma pol}$ scheme are the suggested PBE values for H and C and the same as $DFTB^{hyb}$ for Ag (see also Supporting Information).

3.1. Diatomics dissociation curves

We first computed the $DFTB^{hyb}$ dissociation curves obtained with the ROS and spin-polarized DFTB hamiltonians. Better results were obtained in the spin-polarized case with respect to MRCI results. With the ROS

hamiltonian, binding energies were drastically overestimated for all pairs (not reported), which was expected as DFTB$^{\mathrm{hyb}}$ parameters were extracted including spin-polarization.

The resulting energy curves for the diatomics of interest using the spin-polarized hamiltonian are reported in Figure 2. The corresponding values of the equilibrium distance R_e (in Å) and dissociation energy D_e (in eV) are reported in Table S1. The DFTB$^{\mathrm{hyb}}$ HH and CH dissociation curves are in good agreement with the MRCI ones. In the case of CC, D_e is somewhat underestimated while the R_e value is similar. On the contrary, the AgAg, AgC and AgH D_e values are too large, the largest discrepancy occurring for AgC. D_e values are very satisfactory. By construction, the DFTB$^{\gamma}$ and DFTB$^{\gamma pol}$ curves are essentially superposed with the MRCI curves. However, AgC occurs as a more complex case. Without spin-polarization the DFTB $^4\Sigma^+$ state lies above the $^2\Pi$. Applying the fitting process to the former provide a dissociation energy of 2.04 eV for the latter. This is corrected with the spin-polarized scheme. However, another problem occurs and the DFTB$^{\gamma pol}$ potential is seen to deviate from the MRCI reference at separations beyond the equilibrium distances. This is caused by the larger lowering of the triplet state of carbon in the spin-polarized case *vs* that of the of the doublet of silver. This causes an exaggerated charge transfer from silver to carbon which extends to large interatomic separation, stabilizing the dimer below the neutral separated atoms limit even though the hopping integrals actually vanish. This spurious charge transfer finally disappears for R>11 bohr to join the proper neutral asymptote. The same defect, even increased, is observed with the DFTB$^{\mathrm{hyb}}$ parameterization.

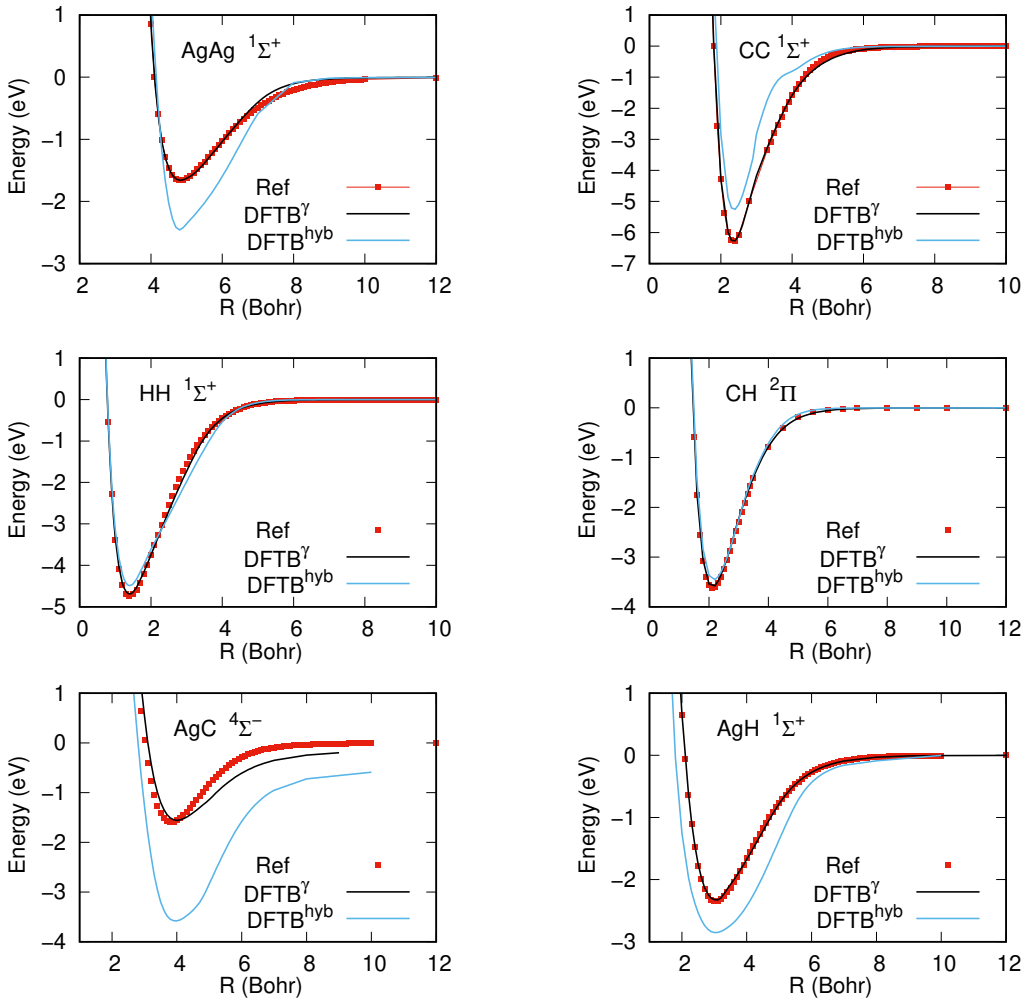

Figure 2: Ground state potential energies curves of X-Y atomic pairs (X,Y=Ag, C, H) as a function of interatomic distances R, obtained with DFTB$^{\gamma pol}$ (black) and DFTB$^{\rm hyb}$ (blue) hamiltonians. The red dots (Ref) indicate the reference potentials (MRCI calculations).

3.2. Benchmark : structures and energetics of Ag_n and Ag_nX (X=C, H)

In this section, we compare the geometries and energetic properties of Ag_n and Ag_nX (X=C, H) clusters determined using DFTB^{hyb}, DFTB$^{\gamma}$ and DFTB$^{\gamma pol}$ parameter sets with those obtained from different DFT functionals or wavefunction methods when available. The available DFTB^{hyb} parameter set was used for both ROS and spin-polarized calculations. DFTB$^{\gamma}$ was used for ROS DFTB calculations consistently with its construction. In this latter parameter set, all SK integral parameters were obtained from the methodology described in Section 2.2 except from the Ag-Ag pair for which the previous improved parameterization by Oliveira and co workers [7] for ROS DFTB was used. The DFTB$^{\gamma pol}$ set of parameters was used for spin-polarized calculations, also consistently with the hamiltonian used for its construction.

3.2.1. Ag_n (n=2-8)

The DFTB structures of Ag_n clusters (n=2-8) obtained with the three parameter sets are similar and similar to the well known DFT stable ones [37, 38]. These structures and the corresponding DFTB cohesion energies per atom are reported in Figure 3 along with other DFT and wavefunction results for comparison (also see Tables S4 and S5 in the Supplementary Information). As can be seen in this figure, DFTB^{hyb} overestimates cohesion energies with respect to several hybrid DFT and correlated wavefunction results. The use of DFTB$^{\gamma}$ considerably improves the results as already shown in ref. [7]. Using the DFTB$^{\gamma pol}$ parameters determined in the present work leads to further decrease of the cohesion energy, leading to values per atom in excellent agreement with CCSD(T) results [39] (see Figure 3 and Table S4).

3.2.2. Ag_nC

The most stable geometries of Ag_nC (n=1-6) determined with the DFTB$^{\gamma}$ (DFTB$^{\gamma pol}$ for n=1,2) and DFTB^{hyb} sets of parameters are reported in Figure 4 along with those optimized with the B3LYP-D3BJ and wB97XD functionals. The energy differences between the two lowest energy isomers are also reported when it is relevant. The corresponding Ag-Ag and Ag-C bond distances are reported in Table S6 and the cohesion energies in Table S7. In all cases, for n>1, the structures of the two lowest energy isomers obtained using the PBE0 functional by Naumkin [42] were used as starting point geometries.

The structures of AgC and Ag_2C were determined with the spin-polarized hamiltonian as their ground electronic states are respectively quartet and

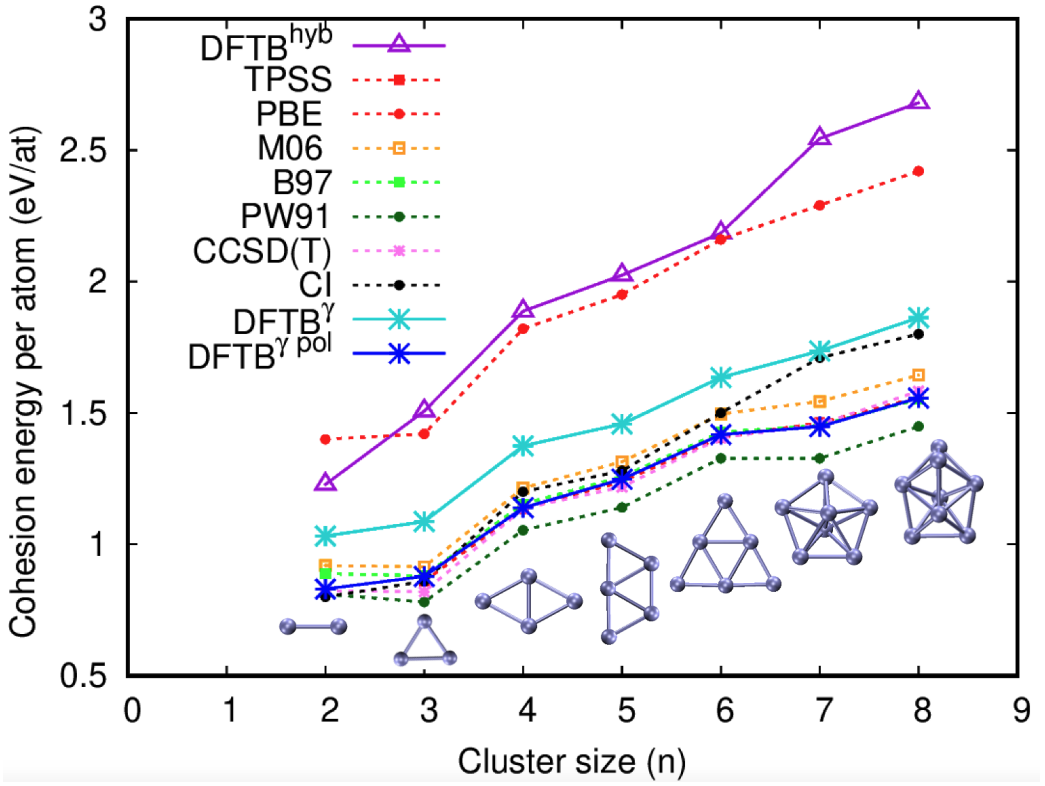

Figure 3: Cohesion energy per atom of Ag_n (n=1-8) clusters with the three parameter sets $\mathrm{DFTB^{hyb}}$ and $\mathrm{DFTB^{\gamma}}$ and $\mathrm{DFTB^{\gamma pol}}$. DFT (TPSS [40], PBE [38], M06 [39] , B97 [39] , PW91 [39]), CCSD(T) [39] and CI [41] results were added for comparison.

triplet spin states [42]. In the AgC dimer, the AgC equilibrium distance is slightly larger with DFTB than at the DFT level. Regarding Ag_2C, both $D_{\infty h}$ and C_{2v} geometries could be optimized but a reverse energetic order was obtained with respect to DFT. At the DFTB level, the AgCAg angle of the C_{2v} structure is smaller than at the DFT level (DFT: 76.3° , DFTB$^{\gamma}$: 69.8°, DFTB$^{\text{hyb}}$: 62.8°) while Ag-Ag distances are shorter and the AgC distances are longer (See Table S6). Interestingly, using the ROS hamiltonian and both DFTB$^{\gamma}$ and DFTB$^{\text{hyb}}$ sets of parameters, the lowest spin-states optimized structures were found as the most stable AgC and Ag_2C isomers, which is not correct (see Table S7) and the linear structure was not obtained in the case of Ag_2C.

Only the structures of Ag_nC (n=3-8) determined with the ROS DFTB hamiltonian are presented for both DFTB$^{\text{hyb}}$ and DFTB$^{\gamma}$ sets of parameters. This can be justified as their electronic ground state is either doublet (n odd) or singlet (n even). Using the spin-polarized hamiltonian, we did not obtain satisfactory results as we noticed an overstabilisation of high-spin states over low-spin states with both DFTB$^{\text{hyb}}$ and DFTB$^{\gamma pol}$ sets of parameters, making the former the most stable geometries, which is not the case in DFT. Besides, regarding low-spin states structures determined with the spin-polarized hamiltonian, the C atom tends to be closer to the Ag atoms even leading to an unexpected structure as the most stable one, which is planar Ag_5C with C at the center of the Ag_5 ring. The possible interpretation is an issue in charge distribution resulting from the questionable description of charge transfer from Ag to C, which is enhanced in the spin-polarized case. For instance, for the Ag_5C isomer reported in Figure 4, the Mulliken charges amount to -0.39 on the C atom and +0.22 on the Ag atom on the other side from the Ag_4 plane (+0.04 on these 4 Ag atoms which are however closer to the C atoms) using the ROS DFTB hamiltonian and the DFTB$^{\gamma}$ parameters. These charges amount to -0.46 and +0.15 respectively in the spin-polarized case (+0.07 on the other Ag atoms). Using the DFTB$^{\text{hyb}}$ parameters, the geometries are similar in both the spin-polarized and non spin-polarized cases along with DFTB$^{\gamma pol}$ parameters. The atomic charge distribution on the Ag_5C isomer reported in Figure 4 amounts to -0.42 on C, -0.009 on the furthest Ag atom and on 0.10 on the 4 Ag atoms in the same plane, which makes more physical sense as charge transfer is more important when the atoms are closer.

Regarding Ag_nC (n=3,4), both C_{2v} and C_{3v} isomers were obtained with

DFTB$^{\gamma}$ and DFTB$^{\text{hyb}}$ sets of parameters. The DFTB$^{\gamma}$ Ag-Ag and AgC distances were found globally in better agreement with the DFT ones than the DFTB$^{\text{hyb}}$ values. In the case of Ag_nC (n=5,6), only one isomer was obtained from the two PBE0 starting point geometries using the DFTB$^{\gamma}$ set of parameters whereas two different structures were obtained with DFTB$^{\text{hyb}}$. However, these two structures considerably differ from the DFT ones. On the opposite, the DFTB$^{\gamma}$ Ag_5C structure has a C_{4v} symmetry and resembles the wB97XD second low lying energy isomer. The DFTB$^{\gamma}$ Ag_6C structure is also similar to the most stable DFT isomer.

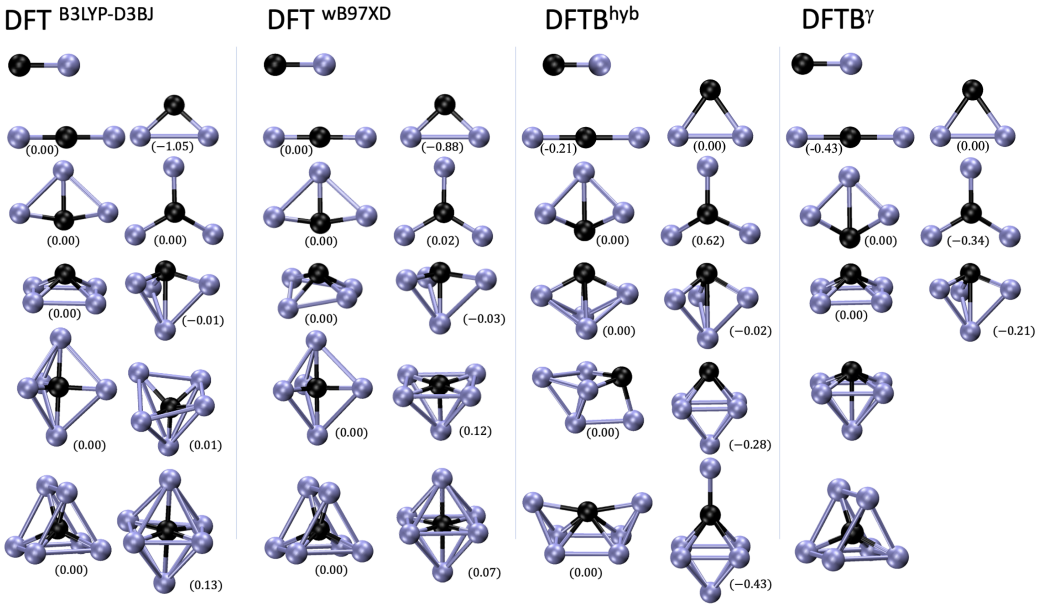

Figure 4: DFT (B3LYP-D3BJ and wB97XD functionals), DFTB$^{\text{hyb}}$ and DFTB$^{\gamma}$ optimized geometries of the lowest energy Ag_nC (n=1-6) isomers in their lowest spin states. Energy differences (in parenthesis in eV) between isomers were also added when relevant.

The evolution of $E^{cohes.}$, BE and $\frac{d^2E}{dn^2}$ as a function of n are reported in Figure 5 a, b and c respectively (also see the corresponding numerical values in Tables S7, S8 and S9 in the Supplementary Information). As can be seen in Figure 5 a, the DFTB$^{\gamma}$ cohesion energies are closer to DFT values than the DFTB$^{\text{hyb}}$ values that are significantly overestimated. It is also the case of binding energies (see Figure 5 b) : DFTB$^{\text{hyb}}$ BEs are greatly overestimated while DFTB$^{\gamma}$ BEs are closer to the DFT ones, even being lower in some case (n=3,4). Regarding the second energy derivatives (Figure 5 c), both

DFTB^{hyb} and DFTB$^{\gamma}$ calculations lead to the same odd-even pattern as the two DFT functionals.

In conclusion to the study of Ag_nC clusters, DFTB$^{\gamma}$ geometries are closer to the DFT ones than DFTB^{hyb} geometries. The energetics are also considerably improved taking DFT values as references. For AgC and Ag_2C which are respectively quartet and triplet spin-states, the use of spin-polarized hamiltonian is mandatory while for the other clusters (n>2) which are either doublet or singlet spin-states, using non spin-polarized ROS DFTB provides better results.

3.2.3. Ag_nH

The most stable geometries of Ag_nH (n=1-7), which are either singlet (n odd) or doublet (n even) spin-states, were determined using the ROS DFTB hamiltonian. The structures optimized using the DFTB$^{\gamma}$ and DFTB^{hyb} sets of parameters alongside those optimized with the B3LYP-D3BJ and wB97XD functionals, are reported in Figure 6. The corresponding internuclear distances are reported in Table S10. The starting-point geometries were retrieved from Zhao et al. [43] and Kuang et al. [44]. In these articles, the geometries were optimized using the PW91PW91 functional in conjunction with two different basis sets. In some cases (n=2,6,7), the most stable isomers were found to be different in Zhao et al. [43] and Kuang et al. [44], revealing the difficulty to determine unambiguously the structure of the most stable Ag_nH isomer.

Overall, for the structures of the clusters that are similar at all levels of theory, the geometrical parameters are similar for the two DFT functionals. The agreement between DFTB$^{\gamma}$, DFTB^{hyb} and DFT Ag-H distances is highly satisfactory for the AgH dimer (1.62 Å vs 1.61 Å). The DFTB$^{\gamma}$ Ag-Ag distances are longer than the DFTB^{hyb} ones, improving the agreement with DFT results although remaining too short. On the opposite, DFTB$^{\gamma}$ Ag-H distances are shorter than the DFTB^{hyb} ones, which also improves the agreement with DFT results (see Table S10).

In the case of Ag_2H, the geometry of the DFTB$^{\gamma}$ structure is an isosceles triangle, resembling the most stable isomer determined by Kuang et al. [44] and Zhao et al. [43] except that the interatomic distances are different (Ag-H:1.87 Å vs 1.73 Å [44] and Ag-Ag:2.43 Å vs 2.39 Å [44]). The isomer optimized with DFTB^{hyb} is also a triangle but with the H atom being much closer to one Ag atom, similarly to the third low-lying energy isomer determined by Kuang et al. [44] but with shorter interatomic distances (Ag-

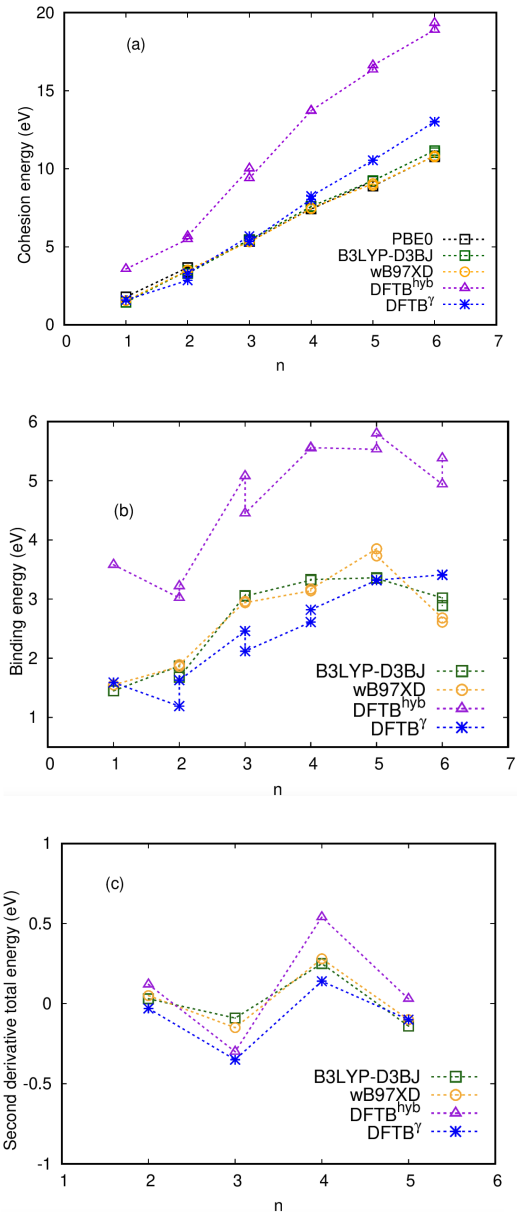

Figure 5: Cohesion energy energy (a), Binding energy (b) and Second derivative total energy (c) of Ag_nC (n=1-6) clusters in DFT with PBE0 [42], wB97XD and B3LYP-D3BJ functionals, DFTB$^{\text{hyb}}$ and DFTB$^{\gamma}$.

H:1.59 Å vs 1.63 Å [44] and Ag-Ag:2.69 Å vs 2.54 Å [44]). The DFTB$^{\gamma}$ and DFTB$^{\mathrm{hyb}}$ structures were obtained whatever the initial position of H in the initial geometries. The most stable B3LYP-D3BJ isomer is also an isosceles triangle but much flatter than those found at the DFTB$^{\gamma}$ and PW91PW91 levels [43, 44]. The wB97XD isomer was found similar to the second low lying isomer obtained by Kuang et al. [44] as the H atom inserts into the Ag dimer.

Regarding Ag_3H, two isomers could be optimized at the DFTB$^{\gamma}$ level (see Figure 6). The geometry of the most stable one differs from that obtained by Kuang et al. [44] by the position of the H atom, which is on top of the Ag_3 triangle at the DFTB$^{\gamma}$ level and in the Ag_3 plane at the PW91PW91 level [44]. At the DFTB$^{\mathrm{hyb}}$ level, only one isomer corresponding to the Ag_3H DFTB$^{\gamma}$ (b) isomer was found. Finally, at both DFT levels considered in the present work, the isomer similar to Ag_3H DFTB$^{\gamma}$ (b) was also found as the most stable, as in Zhao et al. [43]. In the case of Ag_4H, the same trend as for Ag_3H was found at the DFTB$^{\gamma}$ level: one 3D isomer was obtained as the most stable one and not not found at any DFT level. The second low lying DFTB$^{\gamma}$ isomer has a 2D structure, which was found as the only DFTB$^{\mathrm{hyb}}$ isomer and the most stable one with all DFT functionals. In the case of Ag_5H, similar trends were also obtained as the DFT 2D-structures were obtained with both DFTB hamiltonians but the most stable one was found to be a 3D isomer with DFTB$^{\gamma}$ with an important distortion of Ag_5 in the most stable Ag_5H cluster.

Regarding Ag_6H, the most stable isomer was reported to have a 3D structure in the article by Zhao et al. [43] and as a 2D structure in Kuang et al. [44]. With both DFT functionals used in the present work and with the DFTB$^{\mathrm{hyb}}$ hamiltonian, both structures were locally optimized with the 3D structure found as the most stable one. With the DFTB$^{\gamma}$ hamiltonian, the same 2D structure was obtained but two lower energy isomers were optimized. In the most stable one, the H atom interacts with distorted Ag_6 -originally planar for bare silver cluster- structure. In the second low lying energy isomer, the H atom interacts with the other distorted Ag_6 stable 3D isomer (pyramid with a 5-member ring basis).

Finally, in the case of Ag_7H, only 3D structures were found. With the B3LYP-D3BJ and wB97XD functionals the two lowest energy structures were found quasi-degenerated. Each structure was determined as the most stable

one in Zhao et al. [43] and Kuang et al. [44]. The DFTB^{hyb} most stable structure is the second energy one found by Kuang et al. [44] and the second low lying isomer is the one optimized by Zhao et al. [43]. The DFTB$^{\gamma}$ most stable structure was obtained by local optimization of the structure determined by Zhao et al. [43]. The isomer located 0.26 eV above was obtained from the most stable one optimized by Kuang et al. [44]. In this DFTB$^{\gamma}$ isomer, the H atom interacts with 3 Ag atoms rather than 2 at the DFT level.

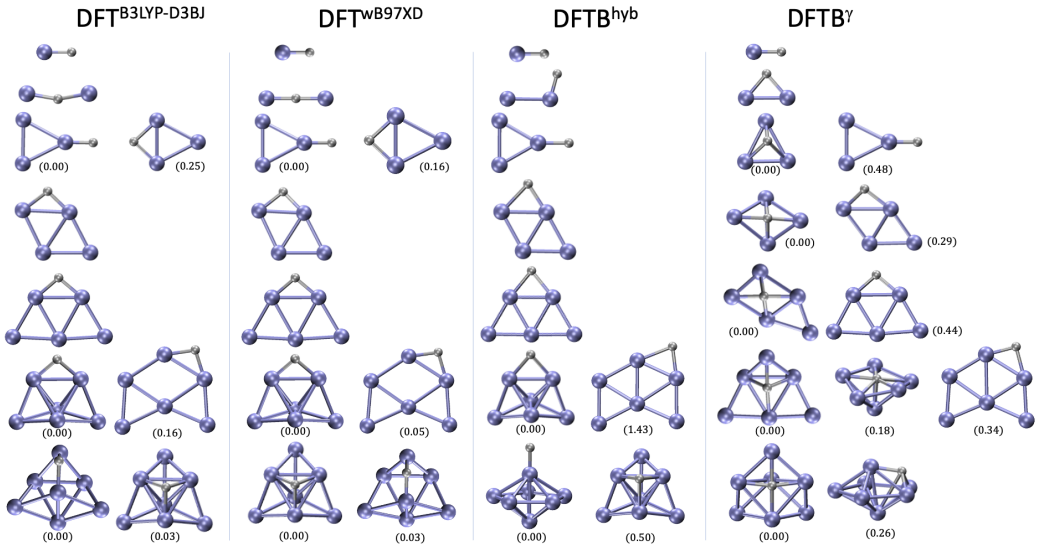

Figure 6: Optimized geometries of Ag_nH (n=1-7) at the DFT (B3LYP-D3BJ and wB97XD functionals) and (DFTB$^{\gamma}$ and DFTB^{hyb}) DFTB levels. When several isomers were computed, their relative energy with respect to the most stable one is specified in parenthesis in eV.

The evolution of E$^{cohes.}$, BE and $\frac{d^2E}{dn^2}$ as a function of n for the most stable isomers of Ag_nH (n=1-6) are reported in Figure 7 a, b and c respectively. The corresponding data are reported in tables S11, S12 and S13 respectively. As can be seen in Figure 7 a, the DFTB$^{\gamma}$ cohesion energies are closer to DFT values than the DFTB^{hyb} values that are significantly overestimated. As can be seen in Figure 7 b, the DFTB^{hyb} binding energies are globally overestimated with respect to the averaged DFT values. It is interesting to note that the BEs quite differ from one functional to another, especially for n=5. On the opposite, the DFTB$^{\gamma}$ BEs are underestimated with respect to averaged DFT values. Interestingly, the well known odd/even pattern is well

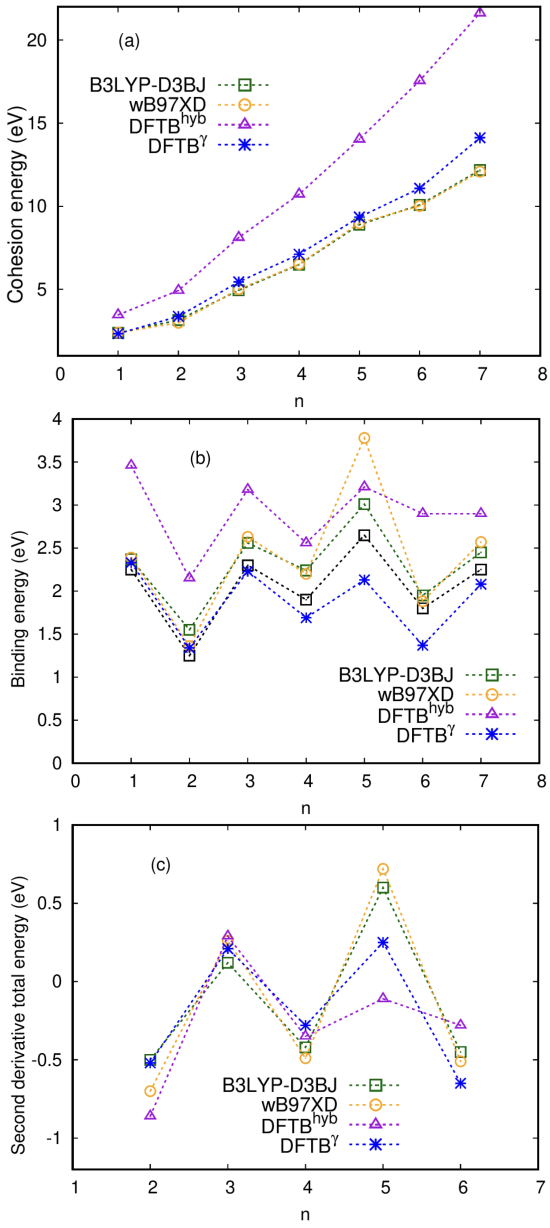

Figure 7: Cohesion energy (a), Binding energy (b) and Second derivative total energy (c) of Ag_nH clusters obtained from DFT (wB97XD and B3LYP-D3BJ functionals) and from $\mathrm{DFTB^{hyb}}$ and $\mathrm{DFTB^{\gamma}}$.

reproduced with DFTB$^{\gamma}$ and up to n=5 for DFTB$^{\mathrm{hyb}}$. Regarding the evolution of the second derivative total energy (Fig. 7 c), the DFT values are well reproduced with DFTB$^{\gamma}$ and, consistently with the BEs evolution, not that well for n=5 in the case of DFTB$^{\mathrm{hyb}}$.

In conclusion to the study of Ag_nH clusters, using DFTB$^{\gamma}$ parameters leads to an improvement of the energetics with respect to DFTB$^{\mathrm{hyb}}$ taking DFT results as references. Regarding the structures, DFTB$^{\gamma}$ leads to better geometries than DFTB$^{\mathrm{hyb}}$ in the case of 2D structures. In the case of 3D structures, the results are not so convincing as the geometries tend to distort during local optimization, the H atom tending to get closer to the Ag atoms. A similar charge transfer issue as for AgC can be invoked although not seen in the diatomics curves. Indeed, in the case of the lowest energy Ag_6H structure for instance, the Mulliken atomic charge on H is -0.46 for DFTB$^{\gamma}$ and -0.14 for DFTB$^{\mathrm{hyb}}$. Regarding the energetics of 2D vs 3D structures, the lowest energy DFTB$^{\gamma}$ isomer tends to adopt a 3D structure for n>2 although it only occurs for n>5 at the DFT level and with DFTB$^{\mathrm{hyb}}$.

Interestingly, the optimization of Ag_6H 3D structure using the spin-polarized version of the hamiltonian and the DFTB$^{\gamma pol}$ set of parameters led to a structure where the H atom enters inside the Ag_n clusters. Using the DFTB$^{\mathrm{hyb}}$ parameters, all structures remain similar as those optimized with the ROS DFTB hamiltonian.

3.3. Application to different types of complexes

This section is dedicated to the study of the transferability of the DFTB$^{\gamma}$, DFTB$^{\gamma pol}$ and DFTB$^{\mathrm{hyb}}$ parameters to systems with different types of chemical bonds involving Ag, C and H atoms. We chose to investigate the structures and energetics of possible intermediates formed by reaction of silver atoms and small clusters with acetylene in a laser vaporisation source or with HMDSO in a plasma source [5], that is to say -(i)- small $Ag_mC_nH_p$ clusters and -(ii)-Ag_n-PAH complexes for the smallest PAH, namely naphthalene $C_{10}H_8$.

3.3.1. $Ag_mC_nH_p$ complexes : structures and energetics

The geometries of a few $Ag_mC_nH_p$ (m=1-3, n=2, p=0-2) clusters were optimized using the B3LYP-D3BJ and wB97XD functionals and the DFTB$^{\mathrm{hyb}}$ and DFTB$^{\gamma}$ hamiltonians using the optimized structures by Bérard et al. [5] as starting point geometries. These structures are either singlet or doublet spin states. The final optimized structures (obtained with the ROS DFTB hamiltonian) are reported in Figure 8. Characteristic bond lengths are reported in Table S14. As can be seen in Figure 8, similar structures were obtained in most cases. Regarding bond distances, DFTB$^{\gamma}$ provides Ag-C, C-C and C-H distances closer to the DFT ones than DFTB$^{\mathrm{hyb}}$ while Ag-Ag distances are too short with both DFTB hamiltonians, with a tendency to be shorter with DFTB$^{\gamma}$. Besides, in the case of $Ag_{1,2}C_2H$ structures, we observed a small distorsion of the geometry with respect to the DFT one. Indeed, the CCH and CCAg angles are slightly smaller than 180°. We may assign this to an overestimation of charge transfer between Ag and C with the DFTB$^{\gamma}$ parameters. For instance, the Mulliken charges on Ag, the two C atoms and H are respectively +0.48, -0.37, -0.25 and +0.12 in AgC_2H (against +0.35, -0.30, -0.20, +0.15 with DFTB$^{\mathrm{hyb}}$). This issue was found worsened using the spin-polarized hamiltonian and the DFTB$^{\gamma pol}$ parameters. We think that this charge transfer issue does not occur with the DFTB$^{\mathrm{hyb}}$ parameters as the Ag-C and Ag-H wells are much deeper.

Cohesion and binding energies for these complexes are reported in Figure 9. The evolution of $E^{cohes.}$ and BE as a function of the complex is similar for all hamiltonians considered in this paper. As can be seen on this figure, similar $E^{cohes.}$ and BE values are found with the two DFT functionals for all complexes. Binding energies for complexes 6 to 8, involving metal-ligand π bonding, are found weak at all levels of theory (below 0.5 eV). On the opposite DFT BEs are found above 2.5 eV for complexes 3 to 5 that involve

covalent metal-ligand bonds. With respect to these DFT data, $DFTB^{hyb}$ values are overestimated and $DFTB^{\gamma}$ values are underestimated.

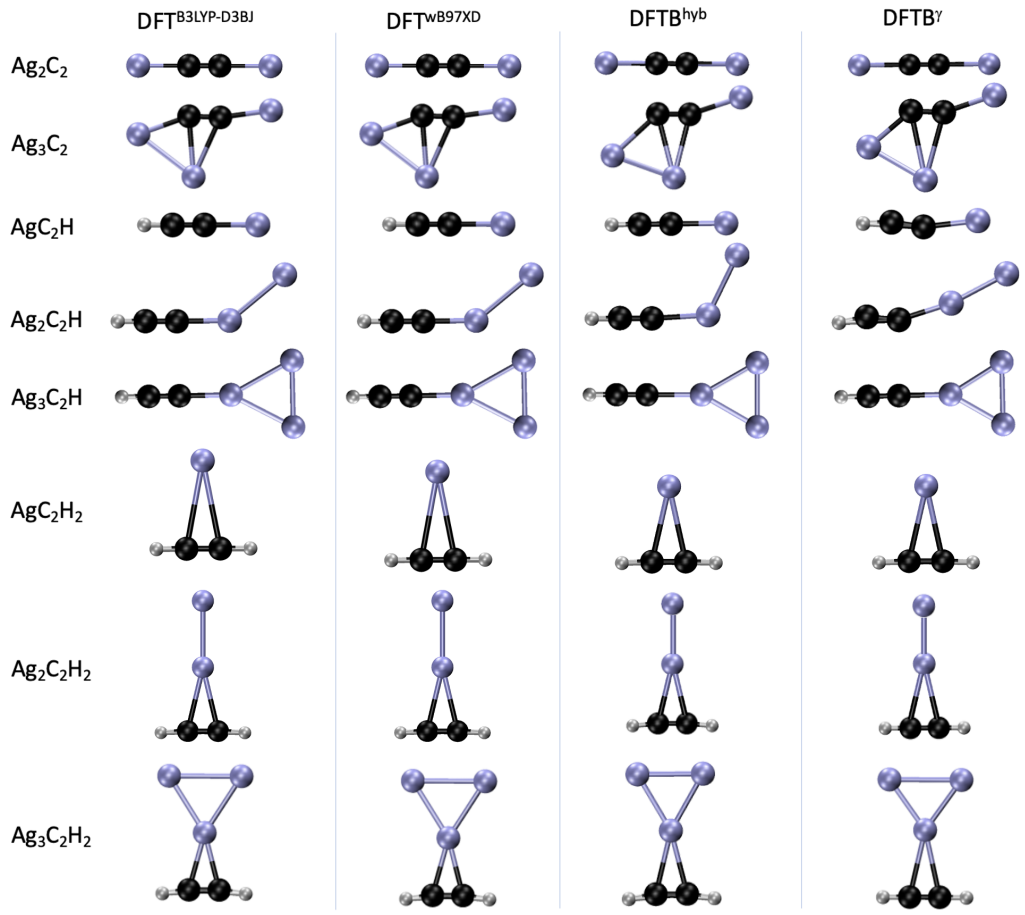

Figure 8: Geometries of $Ag_mC_nH_p$ complexes optimized with DFT B3LYP-D3BJ and wB97XD functionals, ROS DFTB using $DFTB^{hyb}$ and $DFTB^{\gamma}$ sets of parameters.

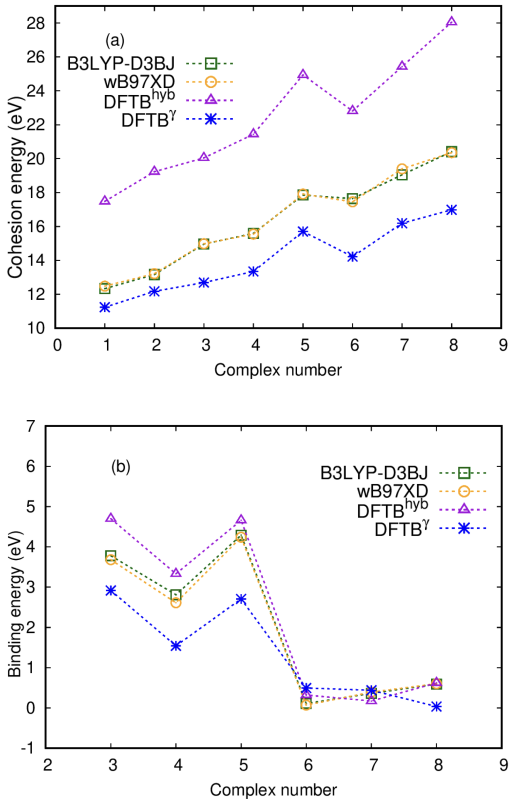

Figure 9: Bond dissociation energies (loss of C_2H for complexes 3-5, loss of C_2H_2 for complexes 6-8) (a) and cohesion energies (b) of $Ag_mC_nH_p$ complexes computed with DFT B3LYP-D3BJ , wB97XD functionals, ROS DFTB with $DFTB^{hyb}$ and $DFTB^{\gamma}$ sets of parameters.

3.3.2. $Ag_nC_{10}H_8$

The last type of systems investigated in this work are $Ag_nC_{10}H_8$ (n=1-8) π complexes. Such Ag_nPAH complexes could be formed in the gas phase and release bare PAHs after reaction with acetylene in laser vaporisation source or with HMDSO in plasma sources [5]. The locally optimized isomers, all obtained from B3LYP-D3BJ starting point geometries, are reported in Figure 10 and the corresponding relevant distances are reported in Table S17. Once again, results obtained with the non spin-polarized ROS DFTB method should be relevant as the complexes of interest are singlet and doublet spin states exclusively.

As can be seen in Figure 10, there is a good agreement between the geometries optimized at the DFT level and the DFTB ones determined with the DFTB$^{\gamma}$ parameters. The only noticeable differences concern $Ag_4C_{10}H_8$ as the silver tetramer is displaced on the side of the naphthalene molecule with DFTB$^{\gamma}$ and the $Ag_8C_{10}H_8$ in which the 3D structure of Ag_8 are different in DFT and DFTB$^{\gamma}$, the Ag_8 structure being that of bare Ag_8 in the DFTB$^{\gamma}$ complex. The structures obtained with the DFTB$^{\text{hyb}}$ parameters present some quite important out-of-plane distortion of the naphthalene molecule for n ranging from 4 to 6 and for n=7 to lesser extent. Besides, with DFTB$^{\text{hyb}}$, the initial structures of Ag_n originally planar, adopt 3D structures upon interaction with naphthalene for n=5,6.

The Ag_n-$C_{10}H_8$ binding energies as a function of n are reported in Figure 11. Using the DFTB$^{\gamma}$ parameters without including dispersion clearly underestimates the BEs with respect to DFT. We added a Grimme D3BJ correction using parameters available in the DFTB+ manual (see Supplementary Information for precisions). We are however aware that in order to be accurate, the parameters of such correction should also be optimized, which we considered out-of-the scope of this work. By adding such dispersion term, the binding energy values obtained with DFTB$^{\gamma}$ parameters becomes closer to the DFT data, unsurprisingly revealing the crucial role of dispersion on the stability of such complexes. On the opposite, using the DFTB$^{\text{hyb}}$ parameters without adding dispersion leads to overstimated BEs with respect to DFT values. Reasonable values are found for n=1-4 and n=7-8. Overestimation however becomes large for n=5-6, consistently with the out-of-plane deformation of the naphthalene molecule.

We optimized the same series of $Ag_nC_{10}H_8$ (n=1-8) complexes using the

spin-polarized hamiltonian that also includes D3BJ Grimme dispersion corrections. The geometries are reported in Figure S2 with the geometrical parameters in Table S19. The BEs are reported in Figure S3 and the values in Table S20. Using the DFTB$^{\gamma pol}$ parameters, structures comparable to the DFT ones were obtained, even for n=8, except for n=2 and 3 where a all the Ag atoms become closer to the PAH plane, suggesting a slight overestimation of dispersion interaction. Regarding the BEs, they are close to the DFT values for n=1,2,4 and larger for n=3, 5-6. However, the trends as a function of n are better than for DFTB$^{\text{hyb}}$ for which similar results as wth the ROS DFTB hamiltonian were obtained.

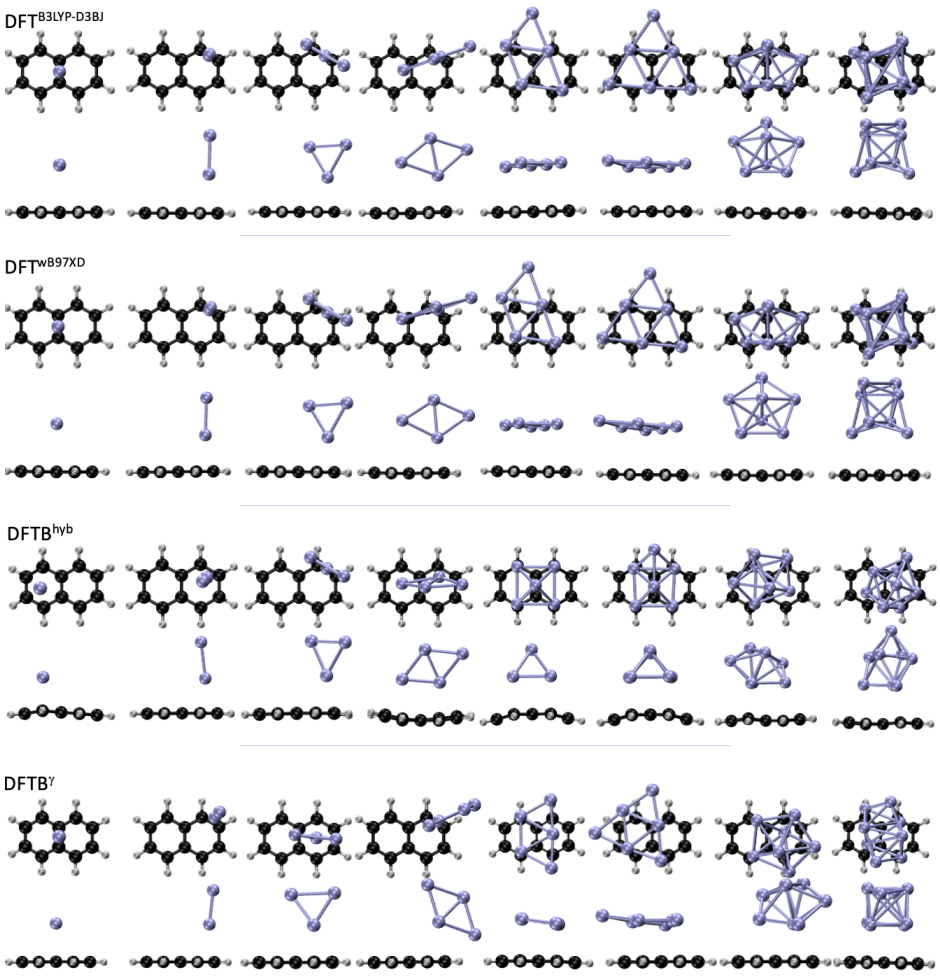

Figure 10: Geometries of $Ag_nC_{10}H_8$ complexes optimized with DFT B3LYP-D3BJ and wB97XD functionals, and $DFTB^{hyb}$ and $DFTB^{\gamma}$ hamiltonians (from top to bottom).

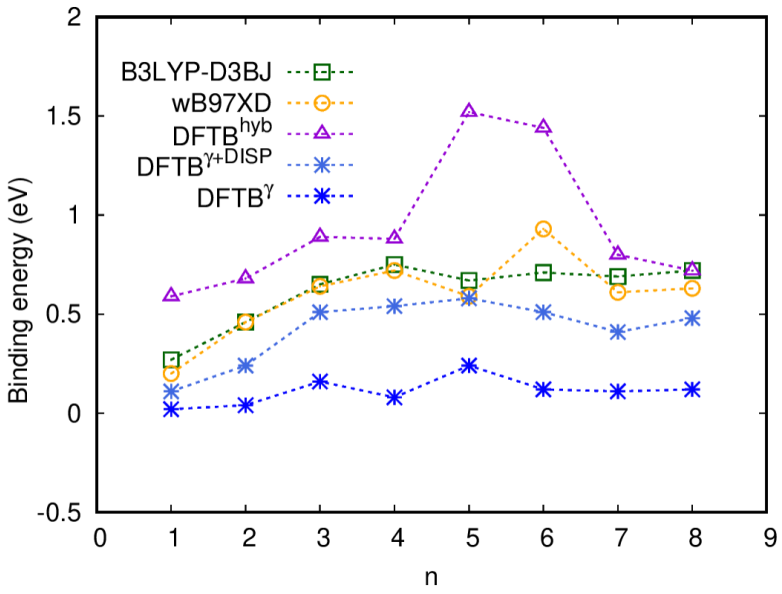

Figure 11: Binding energies (BEs) for $Ag_nC_{10}H_8$ complexes obtained with DFT wB97XD and B3LYP-D3BJ functionals, and $DFTB^{hyb}$ and $DFTB^{\gamma}$ hamiltonians

To conclude on this subsection, using $DFTB^{\gamma pol}$ or $DFTB^{\gamma}$ parameter sets and including dispersion interactions improve the DFTB description of Ag_n-$C_{10}H_8$ clusters with respect to $DFTB^{hyb}$. Our study shows that $DFTB^{\gamma}$ and $DFTB^{\gamma pol}$ both provide a satisfactory description of the geometries of Ag_n-$C_{10}H_8$ clusters with respect to DFT but that including dispersion interaction is needed to obtain metal-ligand binding energies close to the DFT ones. On the opposite, the $DFTB^{hyb}$ leads to questionable geometries and overestimated BEs in some cases but to satisfactory energetic results for several stoichiometries.

4. Conclusions

In this study, we have examined the reliability of the DFTB scheme to describe complexes and clusters made of Ag, C and H atoms. In addition to the currently available DFTB parameters $DFTB^{hyb}$, we propose mew SCC-DFTB parameterization based on DFT SK integrals and recalibration on atomic pairs MRCI calculations for clusters made of Ag, C and H atoms. Two sets of parameters were developed and tested : the $DFTB^{\gamma}$ set of parameters consistent with ROS DFTB calculations and the $DFTB^{\gamma pol}$ set that

does not include dispersion, and that was built for spin-polarized calculations.

These sets of parameters are tested on a variety of $Ag_mC_nH_p$ clusters involving different types of metal-ligand bonds. Locally optimized geometries, cohesion and metal-ligand binding energies are compared to DFT results. Regarding Ag_nX (X=C,H), the DFTB$^{\gamma}$ results are globally in better agreement than DFTB$^{\mathrm{hyb}}$results, in particular regarding the energetics. When coming to $Ag_mC_nH_p$ (m=1-3, n=2, p=0-2) clusters with various types of bonds, both DFTB hamiltonians globally provide good geometries (slightly better with DFTB$^{\gamma}$) but DFTB$^{\gamma}$ underestimates the energetics while it is the opposite for DFTB$^{\mathrm{hyb}}$. Besides, in a few cases ($Ag_{1,2}C_2H$), the geometry is slightly distorted, which is probably due to an overestimation of charge transfer from Ag to C and H.

Finally, in the case of $Ag_nC_{10}H_8$ where the metal-ligand bond involves delocalised electrons, DFTB$^{\gamma}$ provides satisfactory geometries with underestimated binding energies.This can be corrected by adding an empirical dispersion term. In the case of DFTB$^{\mathrm{hyb}}$the results strongly depend on the size of the silver clusters. In some cases, the geometries of naphthalene are distorted with a clearly overestimated binding energy for n=5,6. In the other cases, the geometries are quite satisfactory with an overestimation of the BE that decreases when the silver cluster size increases.

Spin-polarized calculations with the DFTB$^{\gamma pol}$ parameters take spin multiplicity into account and improve the description of atoms in particular. However, they were shown not to improve the results with respect to the ROS DFTB hamiltonian for singlet and doublet spin states clusters except for Ag_n clusters. However, very good results were obtained for triplet and quartet spin-states clusters ($Ag_{1,2}C$) with respect to DFTB$^{\mathrm{hyb}}$in particular regarding the energetics. Let us mention that the spin constants in the spin-polarization scheme introduce supplementary parametric complexity with significant magnitude, which further impacts the transferabilty of the parametrization especially concerning charge transfer.

In conclusion, reaching a satisfactory description of both structures and energetics of complexes and clusters of silver and hydrocarbons at the DFTB level is a challenge. However, our new parameterization scheme globally leads to improve their description with respect to DFT data. Even though we

have not suceedded in developing a unique DFTB parameterization scheme achieving perfect results in all the systems of the investigated benchmark, it appears that the DFTB$^{\gamma}$ pararametrization can be used to obtain an efficient pre-filtering optimization scheme to provide low energy isomer candidates, possibly further refined using DFT for final confirmation. It can also be used to investigate the growth of $Ag_mC_nH_p$ clusters using Monte Carlo or molecular dynamics simulations and in understand the structural, energetical, entropical and dynamical growth patterns governing either segregation or mixing between metallic and organic phases.

Acknowledgements

This work has been funded by the French "Agence Nationale de la Recherche" (ANR), project GROWNANO ANR-21-CE29-0001. The authors thank the computing mesocenter CALMIP ("CALcul en MIdi Pyrénées", UAR3667 of CNRS) for generous allocation of computer resources (project p17002). They also thank Rahma Dahmani for providing DFT results and Nicolas Suaud for complementary wavefunction calculations on AgC dissociation curves.

Appendix A. Supplementary data

Supplementary data to this article can be found online at XXX. Computational details are provided regarding the SCC-DFTB hamiltonians: spin coupling constants, D3 damping function parameters, convergence criteria and electronic energy damping functions (parameters can be found in Table S1 and S2). Details about the wavefunction calculations on the AgC dissociation curve are also specified, dissociation curves are shown in Figure S1 and their characteristics are reported in Table S3.
Table S4 and S5 contains data used to plot cohesion energies of Ag_n clusters in Figure 3.
Table S6 contains geometrical parameters for Ag_nC clusters reported in Figure 4. Tables S7-S9 correspond to the values used in the graphs in Figure 5 for cohesion energy, binding energy and second derivative total energy of Ag_nC respectively.
Table S10 contains geometrical parameters for Ag_nH clusters reported in Figure 6. Tables S11-S13 give the values for Figure 7 : cohesion energy, binding energy and second derivatives total energy of Ag_nH.
Table S14 contains geometrical parameters for $Ag_mC_nH_p$ clusters reported

in Figure 8. Tables S15 and S16 list the cohesion energy values and binding energies of $Ag_mC_nH_p$ corresponding to Figure 9.
Table S17 contains geometrical parameters for Ag_n-$C_{10}H_8$ complexes reported in Figure 10. Table S18 contains the Ag_n-$C_{10}H_8$ binding energy values which are plotted in Figure 11.
The structures of Ag_n-$C_{10}H_8$ clusters optimized with the spin-polarized hamiltonian are reported in Figure S2. The corresponding geometrical parameters are reported in Table S19. Their binding energies are plotted in Figure S3 and the corresponding values are reported in Table S20.
The parameters developed in this article with input examples and optimized geometries are available in a Zenodo repository (doi: 10.5281/zenodo.12544455).

References

[1] I. Chakraborty, T. Pradeep, Atomically precise clusters of noble metals: Emerging link between atoms and nanoparticles, Chem. Rev. 117 (2017) 8208–8271. doi:10.1021/acs.chemrev.6b00769.

[2] R. A. McIntyre, Common nano-materials and their use in real world applications, Sci. Prog. 95 (2012) 1–22. doi:10.3184/003685012X13294715456431.

[3] Y. Zeng, S. Havenridge, M. Gharib, A. Baksi, K. L. D. M. Weerawardene, A. R. Ziefuß, C. Strelow, C. Rehbock, A. Mews, S. Barcikowski, M. M. Kappes, W. J. Parak, C. M. Aikens, I. Chakraborty, Impact of ligands on structural and optical properties of ag29 nanoclusters, J. Am. Chem. Soc. 143 (2021) 9405–9414. doi:10.1021/jacs.1c01799.

[4] A. Chandrasekar, T. Pradeep, Luminescent silver clusters with covalent functionalization of graphene, J. Phys. Chem. C 116 (2012) 14057–14061. doi:10.1021/jp304131v.

[5] R. Bérard, K. Makasheva, K. Demyk, A. Simon, D. Nuñez Reyes, F. Mastrorocco, H. Sabbah, C. Joblin, Impact of Metals on (Star)Dust Chemistry: A Laboratory Astrophysics Approach, Front. astron. space sci. 8 (2021) 654879. doi:10.3389/fspas.2021.654879.

[6] M. Elstner, D. Porezag, G. Jungnickel, J. Elsner, M. Haugk, T. Frauenheim, S. Suhai, G. Seifert, Self-consistent-charge density-functional tight-binding method for simulations of complex materials properties, Phys. Rev. B 58 (1998) 7260–7268. doi:10.1103/PhysRevB.58.7260.

[7] L. F. L. Oliveira, N. Tarrat, J. Cuny, J. Morillo, D. Lemoine, F. Spiegelman, M. Rapacioli, Benchmarking Density Functional Based Tight-Binding for Silver and Gold Materials: From Small Clusters to Bulk, J. Phys. Chem. A 120 (2016) 8469–8483. doi:10.1021/acs.jpca.6b09292.

[8] N. Tarrat, M. Rapacioli, J. Cuny, J. Morillo, J.-L. Heully, F. Spiegelman, Global optimization of neutral and charged 20- and 55-atom silver and gold clusters at the dftb level, Comput. Theor. Chem. 1107 (2017) 102–114. doi:10.1016/j.comptc.2017.01.022.

[9] J. Cuny, N. Tarrat, F. Spiegelman, A. Huguenot, M. Rapacioli, Density-functional tight-binding approach for metal clusters, nanoparticles, surfaces and bulk: application to silver and gold, J. Condens. Matter Phys. 30 (2018) 303001. doi:10.1088/1361-648X/aacd6c.

[10] M. Rapacioli, F. Spiegelman, N. Tarrat, Evidencing the relationship between isomer spectra and melting: the 20- and 55-atom silver and gold cluster cases, Phys. Chem. Chem. Phys. 21 (2019) 24857–24866. doi:10.1039/C9CP03897C.

[11] Z. Liu, F. Alkan, C. M. Aikens, TD-DFTB study of optical properties of silver nanoparticle homodimers and heterodimers, J. Chem. Phys. 153 (2020) 144711. doi:10.1063/5.0025672.

[12] O. A. Douglas-Gallardo, M. Berdakin, T. Frauenheim, C. G. Sánchez, Plasmon-induced hot-carrier generation differences in gold and silver nanoclusters, Nanoscale 11 (2019) 8604–8615. doi:10.1039/C9NR01352K.

[13] D. H. Ziella, M. C. Caputo, P. F. Provasi, Study of geometries and electronic properties of agsin clusters using dft/tb, Int. J. Quantum Chem. 111 (2011) 1680–1693. doi:10.1002/qua.22815.

[14] J. H. Mokkath, U. Schwingenschlögl, Structural and optical properties of si-doped ag clusters, J. Phys. Chem. C 118 (2014) 4885–4889. doi:10.1021/jp4112958.

[15] S. K. Giri, G. C. Schatz, Photodissociation of h2 on ag and au nanoparticles: Effect of size and plasmon versus interband transitions on threshold intensities for dissociation, J. Phys. Chem. C 127 (2023) 4115–4123. doi:10.1021/acs.jpcc.3c00006.

[16] C. Köhler, G. Seifert, T. Frauenheim, Density functional based calculations for Fen (n<32), Chem. Phys. 309 (2005) 23–31. doi:10.1016/j.chemphys.2004.03.034.

[17] M. Elstner, P. Hobza, T. Frauenheim, S. Suhai, E. Kaxiras, Hydrogen bonding and stacking interactions of nucleic acid base pairs: A density-functional-theory based treatment, J. Chem. Phys. 114 (2001) 5149–5155. doi:10.1063/1.1329889.

[18] H. J. Werner, P. J. Knowles, An efficient internally contracted multiconfiguration–reference configuration interaction method, J. Chem. Phys. 89 (1988) 5803. doi:10.1063/1.455556.

[19] D. Porezag, T. Frauenheim, T. Köhler, G. Seifert, R. Kaschner, Construction of tight-binding-like potentials on the basis of density-functional theory: Application to carbon, Phys. Rev. B 51 (1995) 12947–12957. doi:10.1103/PhysRevB.51.12947.

[20] T. Frauenheim, G. Seifert, M. Elstner, T. Niehaus, C. Köhler, M. Amkreutz, M. Sternberg, Z. Hajnal, A. D. Carlo, S. Suhai, Atomistic simulations of complex materials: ground-state and excited-state properties, J. Phys.: Condens. Matter 14 (2002) 3015. doi:10.1088/0953-8984/14/11/313.

[21] C. Köhler, G. Seifert, U. Gerstmann, M. Elstner, H. Overhof, T. Frauenheim, Approximate density-functional calculations of spin densities in large molecular systems and complex solids, Phys. Chem. Chem. Phys. 3 (2001) 5109–5114. doi:10.1039/B105782K.

[22] S. Grimme, J. Antony, S. Ehrlich, H. Krieg, A consistent and accurate ab initio parametrization of density functional dispersion correction (DFT-D) for the 94 elements H-Pu, J. Chem. Phys. 132 (2010) 154104. doi:10.1063/1.3382344.

[23] S. Grimme, S. Ehrlich, L. Goerigk, Effect of the damping function in dispersion corrected density functional theory, J. Comput. Chem. 32 (2011) 1456–1465. doi:10.1002/jcc.21759.

[24] M. Wahiduzzaman, A. F. Oliveira, P. Philipsen, L. Zhechkov, E. van Lenthe, H. A. Witek, T. Heine, Dftb parameters for the periodic table: Part 1, electronic structure, J. Chem. Theor. Comput. 9 (2013) 4006–4017. doi:10.1021/ct4004959.

[25] B. Hourahine, B. Aradi, V. Blum, F. Bonafé, A. Buccheri, C. Camacho, C. Cevallos, M. Y. Deshaye, T. Dumitrică, A. Dominguez, S. Ehlert, M. Elstner, T. van der Heide, J. Hermann, S. Irle, J. J. Kranz, C. Köhler, T. Kowalczyk, T. Kubař, I. S. Lee, V. Lutsker, R. J. Maurer, S. K. Min, I. Mitchell, C. Negre, T. A. Niehaus, A. M. N. Niklasson, A. J. Page, A. Pecchia, G. Penazzi, M. P. Persson, J. Řezáč, C. G. Sánchez, M. Sternberg, M. Stöhr, F. Stuckenberg, A. Tkatchenko, V. W.-z. Yu, T. Frauenheim, DFTB+, a software package for efficient approximate density functional theory based atomistic simulations, J. Chem. Phys. 152 (2020) 124101. doi:10.1063/1.5143190.

[26] H.-J. Werner, P. J. Knowles, G. Knizia, F. R. Manby, M. Schütz, et al., Molpro, version 2015.1, a package of ab initio programs, 2015.

[27] H. Stoll, P. Fuentealba, M. Dolg, J. Flad, L. v. Szentpály, H. Preuss, Cu and Ag as one-valence-electron atoms: Pseudopotential results for Cu2, Ag2, CuH, AgH, and the corresponding cations, J. Chem. Phys. 79 (1983) 5532–5542. doi:10.1063/1.445671.

[28] W. Müller, W. Meyer, Ground-state properties of alkali dimers and their cations (including the elements Li, Na, and K) from ab initio calculations with effective core polarization potentials, J. Chem. Phys. 80 (1984) 3311–3320. doi:10.1063/1.447084.

[29] Z. Li, J. Zhang, D. Meng, Y. Yu, Electronic structure and bonding characters of the two lowest states of copper, silver, and gold monocarbides, Comput. Theor. Chem. 966 (2011) 97–104. doi:10.1016/j.comptc.2011.02.019.

[30] M. J. Frisch, G. W. Trucks, H. B. Schlegel, G. E. Scuseria, M. A. Robb, J. R. Cheeseman, G. Scalmani, V. Barone, G. A. Petersson, H. Nakatsuji, X. Li, M. Caricato, A. V. Marenich, J. Bloino, B. G. Janesko,

R. Gomperts, B. Mennucci, H. P. Hratchian, J. V. Ortiz, A. F. Izmaylov, J. L. Sonnenberg, D. Williams-Young, F. Ding, F. Lipparini, F. Egidi, J. Goings, B. Peng, A. Petrone, T. Henderson, D. Ranasinghe, V. G. Zakrzewski, J. Gao, N. Rega, G. Zheng, W. Liang, M. Hada, M. Ehara, K. Toyota, R. Fukuda, J. Hasegawa, M. Ishida, T. Nakajima, Y. Honda, O. Kitao, H. Nakai, T. Vreven, K. Throssell, J. A. Montgomery, Jr., J. E. Peralta, F. Ogliaro, M. J. Bearpark, J. J. Heyd, E. N. Brothers, K. N. Kudin, V. N. Staroverov, T. A. Keith, R. Kobayashi, J. Normand, K. Raghavachari, A. P. Rendell, J. C. Burant, S. S. Iyengar, J. Tomasi, M. Cossi, J. M. Millam, M. Klene, C. Adamo, R. Cammi, J. W. Ochterski, R. L. Martin, K. Morokuma, O. Farkas, J. B. Foresman, D. J. Fox, Gaussian˜16 Revision C.01, 2016. Gaussian Inc. Wallingford CT.

[31] M. Savoca, T. Wende, L. Jiang, J. Langer, G. Meijer, O. Dopfer, K. R. Asmis, Infrared spectra and structures of silver–pah cation complexes, J. Phys. Chem. Letters 2 (2011) 2052–2056. doi:10.1021/jz2009242.

[32] R. Dahmani, F. Spiegeleman, A. Simon, Dft studies of silver clusters adsorbed on naphthalene: structural, energetic and spectral properties, J. Phys. Chem. A xx (in prep.) xx.

[33] J.-D. Chai, M. Head-Gordon, Long-range corrected hybrid density functionals with damped atom–atom dispersion corrections, Phys. Chem. Chem. Phys. 10 (2008) 6615–6620. doi:10.1039/B810189B.

[34] J. M. L. Martin, A. Sundermann, Correlation consistent valence basis sets for use with the Stuttgart–Dresden–Bonn relativistic effective core potentials: The atoms Ga–Kr and In–Xe, J. Chem. Phys. 114 (2001) 3408–3420. doi:10.1063/1.1337864.

[35] D. Andrae, U. Häußermann, M. Dolg, H. Stoll, H. Preuß, Energy-adjustedab initio pseudopotentials for the second and third row transition elements, Theor. Chem. Acc. 77 (1990) 123–141. doi:10.1007/BF01114537.

[36] K. L. Schuchardt, B. T. Didier, T. Elsethagen, L. Sun, V. Gurumoorthi, J. Chase, J. Li, T. L. Windus, Basis set exchange: a community database for computational sciences, J. Chem. Inf. Model. 47 (2007) 1045–1052. doi:10.1021/ci600510j.

[37] M. Chen, J. E. Dyer, K. Li, D. A. Dixon, Prediction of structures and atomization energies of small silver clusters,(ag) n, n< 100, J. Phys. Chem. A 117 (2013) 8298–8313.

[38] E. M. Fernández, J. M. Soler, I. L. Garzón, L. C. Balbás, Trends in the structure and bonding of noble metal clusters, Phys. Rev. B 70 (2004) 165403.

[39] M. Chen, J. E. Dyer, K. Li, D. A. Dixon, Prediction of structures and atomization energies of small silver clusters, (ag)n, n < 100, J. Phys. Chem. A 117 (2013) 8298–8313. doi:10.1021/jp404493w.

[40] H. Dhillon, R. Fournier, Geometric structure of silver clusters with and without adsorbed cl and hg, Comput. Theor. Chem. 1021 (2013) 26–34. doi:10.1016/j.comptc.2013.06.007.

[41] V. Bonačić-Koutecký, L. Češpiva, P. Fantucci, J. Koutecký, Effective core potential-configuration interaction study of electronic structure and geometry of small neutral and cationic Agn clusters: Predictions and interpretation of measured properties, J. Chem. Phys. 98 (1993) 7981–7994. URL: https://doi.org/10.1063/1.464552. doi:10.1063/1.464552.

[42] F. Y. Naumkin, Shape and property alteration of small silver clusters via doping by carbon: CAg_n (n≤6), Comput. Theor. Chem. 1021 (2013) 191–196. doi:10.1016/j.comptc.2013.07.018.

[43] S. Zhao, Z.-P. Liu, Z.-H. Li, W.-N. Wang, K.-N. Fan, Density functional study of small neutral and charged silver cluster hydrides, J. Phys. Chem. A 110 (2006) 11537–11542. doi:10.1021/jp062985y.

[44] X. Kuang, X. Wang, G. Liu, A density functional theory study on the AgnH (n=1–10) clusters, Struct. Chem. 22 (2011) 517–524. doi:10.1007/s11224-010-9716-5.